Impact of physical layer impairments on C+L-band metro networks

Filipa F. Gomes[1],Luís G. Cancela[1,2]and João L. Rebola[1,2]
[1]*Optical Communications and Photonics Group, Instituto de Telecomunicações, Lisbon, Portugal*
[2]*Department of Information Science and Technology, Instituto Universitário de Lisboa (ISCTE-IUL), Portugal*
{*ffgsa, luis.cancela, joao.rebola*}*@iscte-iul.pt*

Keywords: ASE noise, In-band crosstalk, Metro networks, Multi-band transmission, Nonlinear interference noise

Abstract: To ensure future data traffic capacities, multi-band transmission in optical networks is being proposed, by adding wavelength division multiplexing channels in the L-band to the existing C-band channels. In this work, we study the filterless drop and waste amplified and unamplified solutions used in metro networks with L-band tributary nodes. The cost and power consumption of these nodes is evaluated, as well as the impact of several physical layer impairments on the network performance. In amplified solutions, we show that L-band networks with 9 tributary nodes are feasible, being the optical signal-to-noise ratio achieved when considering amplifiers noise and fiber non-linear interference above 14 dB. In unamplified solutions, to fullfil the power budget, frequency reuse should be used between spans. We show that the in-band crosstalk caused by this frequency reuse leads to 1.5 dB power budget degradation, for a crosstalk level of -20 dB.

1 INTRODUCTION

To offer the best Internet experience, nowadays, it is necessary to resort to cloud services which, in the future, will probably saturate the transport capacity of existing metro networks. Several solutions based on multi-band transmission are being investigated to overcome this possible capacity crunch (Ferrari et al., 2020), but the introduction of the L-band (by adding wavelength division multiplexing (WDM) channels) opens the opportunity for cheaper solutions than placing several fibres in parallel.

Filterless solutions, both amplified and unamplified, are being proposed to reduce even more the cost of upgrading the optical networks to the L-band (Emmerich et al., 2020b), (Paolucci et al., 2020). In particular, the filterless solution is usually applied to networks with horseshoe topology (Emmerich et al., 2020b). In (Paolucci et al., 2020), the L-band filterless unamplified solution is proposed, but due to frequency reuse, in-band crosstalk becomes a relevant impairment that degrades the network performance. As this solution is only suitable for short-reach spans, noise from the amplifiers and fiber non-linearities can be neglected. Due to the impossibility of reusing frequencies in the amplified solution, amplified spontaneous emission (ASE) noise and fiber non-linear interference (NLI) become the main impairments that degrade the network performance.

In all these works, regarding filterless L-band transmission, we have seen that they resort on experimental results and simulations to study the upgrade of the metro area networks. However, an analytical study of the filterless solutions has not been performed in these works.

In this work, we analyse the node components and architectures for the C+L-band, and their cost and power consumption are estimated. A simple analytical formalism of the various physical layer impairments (PLIs) that affect the performance of the filterless solution, either amplified or unamplified, in the horseshoe topology is provided. The impact of ASE noise and NLI on the optical signal-to-noise ratio (OSNR) of the horsehoe topology is studied for filterless L-band amplified solutions and the influence of in-band crosstalk on the electrical signal-to-noise ratio (SNR) is assessed for unamplified solutions.

This work is organized as follows. In section 2, we review the L-band node architectures amplified and unamplified solutions for the C+L transmission. In section 3, we perform an analysis regarding the L-band hardware cost and power consumption. In section 4, the several PLIs that impair the L-band nodes network performance are studied for the amplified and unamplified solutions. In section 5, the final conclusions are drawn.

2 NODE ARCHITECTURE FOR C+L-BAND

Several solutions regarding metro networks with C+L band transmission rely on the horseshoe network topology to manage the access/metro network data traffic (Paolucci et al., 2020). The horseshoe topology is usually composed of two hub nodes (which are nodes that communicate in a meshed topology with other hub nodes) and several tributary nodes (which are nodes that connect with the hub nodes or other tributary nodes, and perform the interface with access metro networks) (Paolucci et al., 2020), (Emmerich et al., 2020a). As shown in Fig. 1, a C+L tributary node architecture has two independent structures, one for C-band signals and other for L-band signals (Emmerich et al., 2020a). These two bands are separated/aggregated by a C/L band filter at the input/output of the node, which typically provides high bands isolation and low insertion losses, introducing a 300 to 500 GHz gap between the C and L bands. The separated L-band solution causes a minimum disruption with pre-existing metro networks working only in the C-band (Emmerich et al., 2020a).

The node configuration used for the C-band, which is shown at the top of Fig. 1 (blue color), can be implemented with various nodes architectures such as filterless drop and waste (FD&W), fixed optical add/drop multiplexers (FOADM) and reconfigurable optical add/drop multiplexer (ROADM) solutions (Emmerich et al., 2020a).

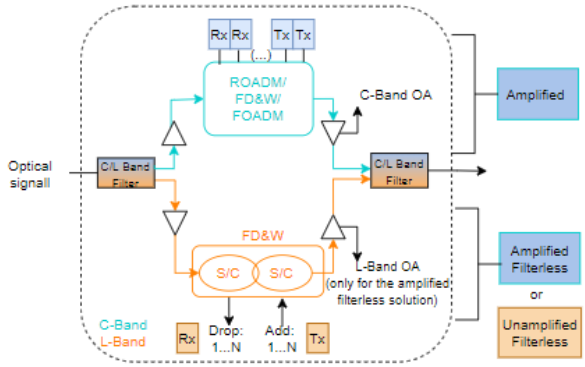

Figure 1: Tributary C+L-band node configuration.

The node configuration for the L-band is shown at the bottom of Fig. 1 (orange color). It is based only on the FD&W solution, whose architecture relies only on splitter/couplers (S/Cs), and can be either amplified or unamplified (Emmerich et al., 2020a). This solution has no filtering in the tributary nodes, which means that when a wavelength is added to the network, it remains in the network until the hub node removes it (amplified solution) or until it is reused once again in the network (unamplified solution) (Emmerich et al., 2020b), (Paolucci et al., 2020). The hub node L-band structure typically uses ROADMs as in the C-band structure counterpart (Hernandez et al., 2020).

2.1 L-band amplified solution

In the amplified solution, there are optical amplifiers (OAs) inside the node before and after the FD&W block, see Fig. 1 (Paolucci et al., 2020).

Fig. 2 presents a possible wavelength planning for the amplified solution in the L-band in a horseshoe topology, where each tributary node has a specific wavelength to communicate with the hub node. This solution does not allow the reuse of frequencies inside the network since each wavelength can only be extracted by the hub node (represented in pink in Fig. 2). The tributary nodes (represented in green in Fig. 2) do not have such capacity since they are based on S/Cs. In Fig. 2, the pink wavelength λ_5 is assigned to the connection between the hub node 1 and the tributary node *E*, but node *E* can not remove this wavelength, which is only removed from the network at the hub node 2. This path is represented by the dashed pink line, and represents a wasted wavelength for nodes F to I (Emmerich et al., 2020a).

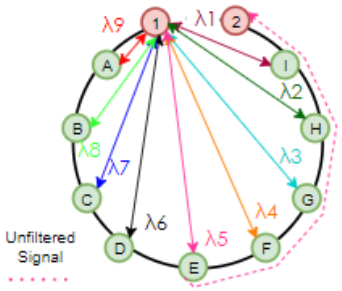

Figure 2: Amplified filterless solution with no frequency reuse for the horseshoe topology. Only the L-band wavelength assignment for the downlink transmission is depicted.

2.2 L-band unamplified solution

The main goal of the L-band unamplified solution is to reduce the nodes cost by not using OAs. This solution limits the L-band transmission distance to adjacent nodes or near adjacent nodes (Emmerich et al., 2020a).

Fig. 3 shows an example of a wavelengh assignment for the unamplified solution, to illustrate a wavelength reuse possibility. As shown in Fig. 3, the wavelength λ_2 is reused in the next-hop and λ_1 is reused

after one hop. As the WDM channel is not amplified, it arrives to the next node with very low power, meaning that a new channel with the same wavelength can be used. However, the (even weak) power leakage on node H can impair the new channel leading to in-band crosstalk. (Emmerich et al., 2020b).

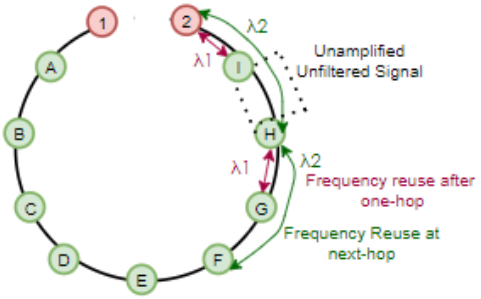

Figure 3: Unamplified filterless solution with frequency reuse for the horseshoe topology. Only the L-band wavelength assignment for the downlink transmission is depicted.

2.3 L-band nodes architectures

In the L-band, the tributary nodes use a FD&W architecture, while the hub nodes have usually a colorless and directionless (CD) ROADM route and select (R&S) architecture, as shown, respectively, in Figs. 4 and 5.

In Fig. 4, the tributary node architecture considers the transmission of 70 WDM channels with a 100 GHz channel spacing in each fiber direction. For two directions and a add/drop (A/D) ratio of 20%, the number of required coherent detection transponders in each L-band node is 28. Thus, beside considering two C/L filters to separate/aggregate the two bands and two amplifiers per node (in the case of the amplified solution), each tributary FD&W node has four S/Cs 1:2, four S/C 1:16, each with 4 unused channels and 28 transponders, as shown in Fig. 4.

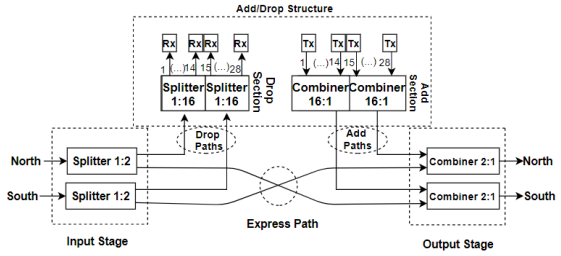

Figure 4: 2-Degree FD&W tributary node.

In Fig. 5, we consider that each 5-degree hub node is connected to 3 different hub nodes and two tributary nodes. So, for an A/D ratio of 20%, a total of 112 wavelengths must be added/dropped in each hub node. As wavelength selective switches (WSSs) with maximum dimension of 1:20 are considered (Hernandez et al., 2020), it is necessary to use 6 cards in the A/D structure to achieve this number of wavelengths. To connect each A/D card to the ROADM input/output directions, express WSSs 1:20 are considered. So, in Fig. 5, the hub node has five WSSs 1:20 at the input and output stages, twelve WSSs 1:20 in the A/D structure, six WSSs 1:8 at the drop section, six S/Cs 1:8 at the add section and 112 transponders.

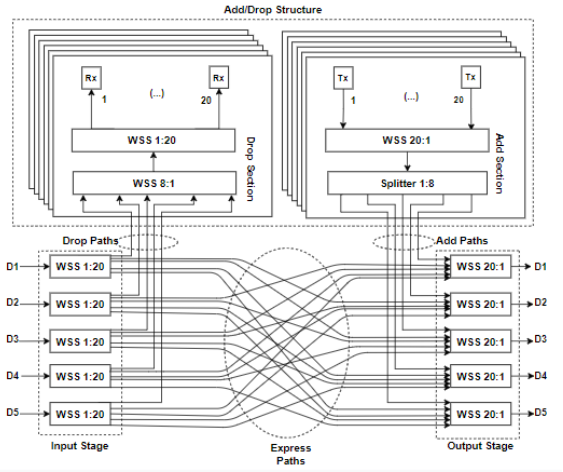

Figure 5: 5-Degree CD ROADM R&S hub node.

3 HARDWARE COST AND POWER CONSUMPTION

In this section, an analysis regarding the cost, power consumption and total offered capacity of an horseshoe topology with 2 hub nodes and 9 tributary nodes (as shown in Fig. 2) is performed and presented in Tab. 1. The analysis is performed considering that the cost and power consumption of the hardware components in the L-band is twice the C-band components cost, which is taken from (Hernandez et al., 2020). The cost is normalized to the cost of a 10 Gbps transponder, whose price is around 330 € (Hernandez et al., 2020).

For comparison purposes, the cost and power consumption of the same horseshoe network have been calculated for the C-band FD&W solution considering the components presented in (Hernandez et al., 2020), and the same A/D ratio of 20%.

The total capacity per fiber reaching the tributary and hub nodes in the L-band is, respectively, 7 Tbps and 28 Tbps, determined from the number of WDM

channels and the transponder capacity, which is, respectively, 70 channels and 100 Gbps for the tributary node and, respectively, 140 channels and 200 Gbps between hub nodes. The total capacity per node presented corresponds to the capacity per A/D structure. So, the capacity per tributary node is 2.8 Tbps and the average total capacity per hub node is calculated considering that 2/5 of the transponders are working at 100 Gbps (to communicate with tributary nodes) and the other 3/5 are at 200 Gbps (to communicate with other hub nodes). Hence, the average total capacity per hub node is 17.9 Tbps.

Table 1: Total cost, power consumption and capacity of the hub and tributary nodes and per horseshoe network.

Cost/Consumption	Node architecture
	Hub
Normalized cost/node	1952.44
Power consumption/node [kW]	18.96
Total capacity/node [Tbps]	17.9
	Trib. Amplified
Normalized cost/node	282.2
Power consumption/node [kW]	3.43
Total capacity/node [Tbps]	2.8
Total cost/horseshoe [k]	6.45
Total pow.cons./horseshoe [kW]	68.75
	Trib. Unamplified
Normalized cost/node	280.95
Power consumption/node [kW]	3.36
Total capacity/node [Tbps]	2.8
Total cost/horseshoe [k]	6.43
Total pow.cons./horseshoe [kW]	68.15

The tributary node unamplified solution is cheaper (less 1.25 of normalized cost) and spends less power per node (around 20 W) than the tributary node amplified solution. The difference between these solutions is only due to the existence or not of OAs. The components that most contribute, around 99%, to the final cost of the node are the transponders. The normalized cost per tributary node is around 3.5 times higher than in the C-band. This occurs because, in the L-band, the number of transponders is almost the double. The power consumption of the tributary node is 3.4 kW, which is around 1.7 times higher than the consumption of the FD&W for the C-band. Other components, such as the S/Cs have a small contribution to the final cost.

The hub node has a normalized cost around 3.5 times higher than the C-band node cost. The power consumption is also around 3.2 times higher than the corresponding C-band node power consumption.

So, the estimated total network cost using FD&W with amplified and unamplified soutions is 2134 k€ and 2128.3 k€, respectively, when the components are twice expensive, which means that the unamplified solution is 0.3% cheaper than the amplified one.

4 PHYSICAL LAYER IMPAIRMENTS IN THE L-BAND

In this section, the analysis of several PLIs, originated inside the nodes as well as in fiber transmission, such as insertion losses, ASE noise, NLI noise and in-band crosstalk is performed, considering quadrature phase-shift keying (QPSK) signal transmission in the L-band. The PLIs impact is quantified by the optical signal-to-noise-ratio (OSNR) given by (Semrau et al., 2019):

$$osnr = \frac{p_{Rx}}{p_{n,ASE} + p_{NLI}} \quad (1)$$

where p_{Rx} is the average signal power at the optical receiver input, $p_{n,ASE}$ is the accumulated ASE noise power and p_{NLI} is the NLI power at the receiver input. The following parameters are considered: the amplifiers noise figure (F_n) is 6.5 dB, at most 0.5 dB higher than in C-band (Correia et al., 2021). The fiber non-linear coefficient in the L-band, $\gamma = 1.2$ W/km, is slightly lower than in the C-band (Semrau et al., 2018), and the attenuation coefficient is α=0.25 dB/km, slightly higher than in the C-band. The channel bandwidth of 26.75 GHz is equal to the symbol rate, R_s, and the WDM channel spacing is 100 GHz.

Fig. 6 represents the spectral occupancy of the 70 channels belonging to the L-band and of the 40 C-band channels, considering the International Telecommunication Union (ITU)-T 100 GHz channel grid (Telecommunication Standardization Sector of ITU, 2020). The L-band central frequency is 188 THz, while, in the C-band, is 193.7 THz. A band gap of 300 GHz between the C and L bands is considered, which contains 3 unused channels.

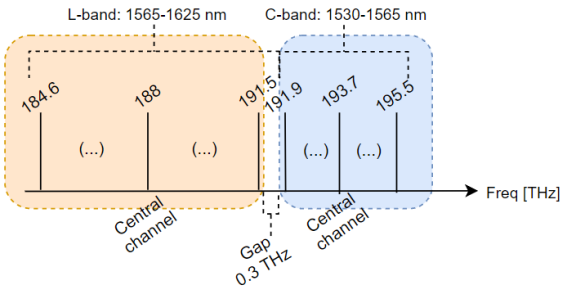

Figure 6: WDM signal frequencies for the C+L-band with 100 GHz channel spacing following the ITU-T grid, considering 40 channels for C-band and 70 channels for L-band.

Regarding the optical filtering effect in the L-band, only the WSSs in the hub nodes contribute to this effect. Hence, the effect of the optical filtering is neglected in the following analysis.

4.1 Insertion losses in amplified and unamplified solutions

In this section, we present the insertion losses of the amplified and unamplified solutions. The losses of each hardware element are those considered in (Hernandez et al., 2020). The WSS losses, which are independent of the WSS size are 7 dB (Sequeira et al., 2021). The insertion losses considered for the S/Cs 1:2, 1:4, 1:8 and 1:16, are respectively, 4, 7, 11 and 15 dB (Inc., 2019). The losses of the C/L band filters are around 0.6 dB (Fiberdyne labs, 2021). The connectors and splices losses are neglected.

In Tab. 2, the insertion losses inside the add, drop and express paths of the tributary and hub nodes are shown. The fiber losses after 10 km are 2.5 dB. The hub node leads to the highest losses, 25 dB. For the tributary node, the add and drop paths losses are the same, 19.6 dB.

Table 2: Insertion losses in the L-band, of the tributary node the hub node.

	Tributary node
Add_{path}	S/C 16:1+S/C 2:1+C/L filter=19.6 dB
$Drop_{path}$	S/C 1:2+S/C 1:16+C/L filter=19.6 dB
$Express_{path}$	S/C 1:2 +S/C 2:1 + 2 ×C/L filter=9.2 dB
	Hub node
Add_{path}	WSS 20:1+S/C 1:8+WSS 20:1=25 dB
$Drop_{path}$	WSS 1:20 +WSS 1:8+WSS 1:20=21 dB
$Express_{path}$	WSS 1:20 +WSS 20:1=14 dB
10 km fiber	2.5 dB

The amplifier gains are designed to perfectly compensate the insertion losses of the worst path inside the node, the add path. For tributary nodes, only pre-amplification is used and the amplifier gain is 22.1 dB to compensate the losses of the 10 km span and node losses.

4.2 ASE noise in the amplified solution

In this section, the accumulated ASE noise power is calculated for the amplified solution in the L-band, considering two worst paths in the horseshoe network, 1) channel insertion at the hub node 1 and drop at node I in Fig. 2, and 2) channel insertion at node A and drop at hub node 2. The accumulation of ASE noise is quantified by the OSNR using (1), firstly, considering the absence of NLI.

The accumulated ASE noise power is given by:

$$p_{n,ASE} = 2 \times \sum_{i=1}^{n_{spans}} [p_{ASE,pre,i} + p_{ASE,pos,i}] \quad (2)$$

where n_{spans} is the number of spans, $p_{ASE,pre,i}$ is the ASE noise power per polarization generated at each i-th pre-amplifier output and $p_{ASE,pos,i}$ is the ASE noise power per polarization generated at each i-th post-amplifier output. The ASE noise power of each amplifier is given by

$$p_{ASE,m,i} = \frac{f_{n,m,i}}{2} \times (g_{m,i} - 1) \times h \times \nu_0 \times R_s \quad (3)$$

where m=*pre* or *pos*, h is the Planck's constant and ν_0 is the optical frequency. The ASE noise power as a function of the channel frequency (in lowpass equivalent definition) after nine spans of the horseshoe network for the cases of channel insertion at tributary node A and hub node 1 is shown in Fig. 7. The ASE noise power increases slightly with frequency and the difference between first and last channel frequencies is less than 0.3 dB. The ASE noise power is about 0.7 dB higher, when the channel insertion is in the tributary node in comparison with insertion in the hub node.

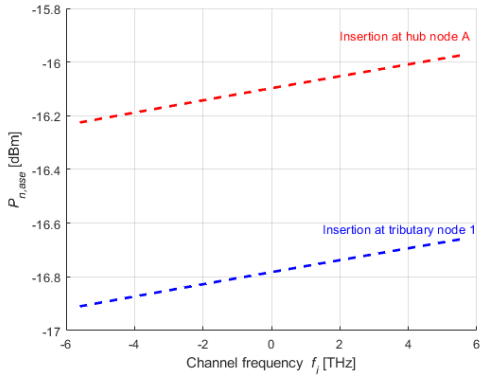

Figure 7: Accumulated ASE noise power as a function of the channel frequency after 9 spans of the horseshoe network for channel insertion in hub 1 and tributary A nodes.

Fig. 8 shows the OSNR evolution along the network, for both cases of signal insertion, for the channel frequency of 188 THz. When signal insertion occurs at node 1, the OSNR is significantly degraded as the signal crosses the nodes, decreasing 9.3 dB. For signal insertion at node A, the OSNR decreases 7.1 dB. The minimum reference OSNR is 8.5 dB to achieve a target BER 4×10^{-3} (Sambo et al., 2020). Fig. 8 shows that, for both cases of signal insertion, the OSNR achieved at the optical receiver input provides a good safety margin in relation to the minimum OSNR.

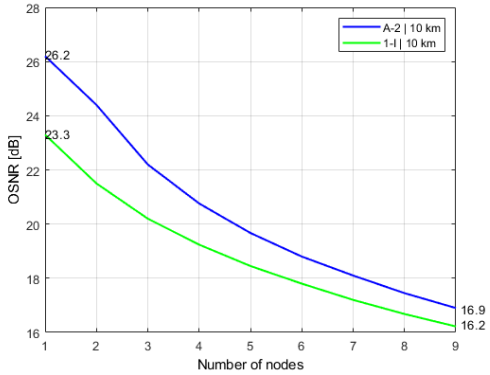

Figure 8: OSNR in the horseshoe topology, for signal insertion at the tributary node A and signal insertion at the hub node 1 for p_{Rx}=0 dBm.

4.3 NLI in the amplified solution

In this section, the NLI noise power and the associated OSNRs are studied for the amplified solution. To perform these studies, the NLI calculation and the OSNR formulation must take into account the presence of inter-channel Stimulated Raman Scattering (SRS). In this section, the Gaussian noise model presented in (Semrau et al., 2019) is considered, where the effect of the SRS in the NLI noise is taken into account in simplified closed-form expressions.

The NLI parameter in the L-band, used in the calculation of the OSNR, is given by (Semrau et al., 2019)

$$\eta(f_i) \approx \sum_{j=1}^{n_{spans}} \left[\frac{P_{i,j}}{P_i}\right]^2 [\eta_{SPM,j}(f_i) n_{spans}^{\varepsilon} + \eta_{XPM,j}(f_i)] \tag{4}$$

where $\eta_{SPM,j}(f_i)$ is the self-phase modulation (SPM) contribution generated in j-th span at frequency f_i, $\eta_{XPM,j}(f_i)$ is the total cross-phase modulation (XPM) contribution generated in j-th span, and $P_{i,j}$ is the power of i-th channel launched into the j-th span, and ε is the coherent factor of NLI accumulation along multiple fiber spans. In this work, as we consider exact loss compensation, $P_{i,j}$=P_i, and NLI coherent accumulation is assumed. The SPM contribution is given by (Semrau et al., 2019):

$$\begin{aligned}\eta_{SPM}(f_i) &\approx \frac{4}{9}\frac{\gamma^2}{B_i^2}\frac{\pi}{\Phi_i \overline{\alpha}(2\alpha+\overline{\alpha})} \\ &\cdot \left[\frac{T_i-\alpha^2}{\alpha}\operatorname{arcsinh}\left(\frac{\Phi_i B_i^2}{\pi\alpha}\right) \right. \\ &\left. + \frac{A^2-T_i}{A}\operatorname{arcsinh}\left(\frac{\Phi_i B_i^2}{\pi A}\right)\right]\end{aligned} \tag{5}$$

where Φ_i=$\frac{3}{2}$ π^2 (β_2+ 2π β_3 f_i), β_2 is the group-velocity dispersion and β_3 is the higher order dispersion parameter (Agrawal, 2010), A= $\alpha+\overline{\alpha}$ and $T_i=(\alpha+\overline{\alpha}-P_{tot}C_r f_i)^2$, where P_{tot} is the WDM signal launch power, B_i is the bandwidth of the i-th channel and C_r is the slope of the linear regression of the normalized Raman gain spectrum (Semrau et al., 2019). The total XPM contribution is given by (Semrau et al., 2019)

$$\begin{aligned}\eta_{XPM}(f_i) &\approx \frac{32}{27}\sum_{k=1,k\neq i}^{N_{ch}}\left(\frac{P_k}{P_i}\right)^2 \frac{\gamma^2}{B_k \Phi_{i,k}\overline{\alpha}(2\alpha+\overline{\alpha})} \cdot \\ &\left[\frac{T_k-\alpha^2}{\alpha}\arctan\left(\frac{\Phi_{i,k}B_i}{\alpha}\right)\right. \\ &\left. + \frac{A^2-T_k}{A}\arctan\left(\frac{\Phi_{i,k}B_i}{A}\right)\right]\end{aligned} \tag{6}$$

where $\Phi_{i,k}=2\pi^2(f_k-f_i)[\beta_2+\pi\beta_3(f_i+f_k)]$. In this work, we consider the simplified case of $\alpha=\overline{\alpha}$.

For the NLI study, C_r=0.028 1/W/km/THz, the dispersion parameter is 17 ps/nm/km and the dispersion slope is ps/nm^2/km. In Fig. 9 (a), the NLI parameter as a function of the WDM channels frequency is shown, for several input powers per channel, considering the horseshoe topology with 9 tributary nodes and 10 km spans. Fig. 9 (a) reveals that, for higher channel input power, the higher the NLI parameter and the steepest its tilt, due to the stronger power transfer from higher to lower frequencies caused by SRS.

In Fig. 9 (b), the corresponding NLI power as a function of the WDM channels frequency is shown. The NLI power is determined by $p_{NLI}=\frac{P_{rx}^3}{\eta}$ (Semrau et al., 2019), As can be observed in Fig. 9 (b), the NLI power increases almost 5 dB, for a 4 dBm power channel, as the channel frequency decreases from the highest to the lowest channels. Also, it can be observed that, as the input power decreases, the NLI power increase is smoother from the highest to the lowest frequency channel. For the -2 dBm channel power, the NLI power remains practically constant for all frequency channels due to the reduced SRS. Notice that the results presented for the NLI power are independent on where the signal is inserted in the network.

The OSNR as a function of the channel frequency after 9 spans considering the ASE noise power and NLI is shown in Fig. 10, for several input channel powers, including the optimal power per channel, which leads to the best OSNR, and the maximum power per channel to comply the minimum OSNR,

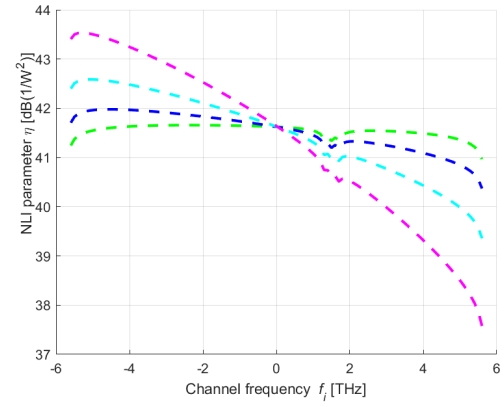

(a)

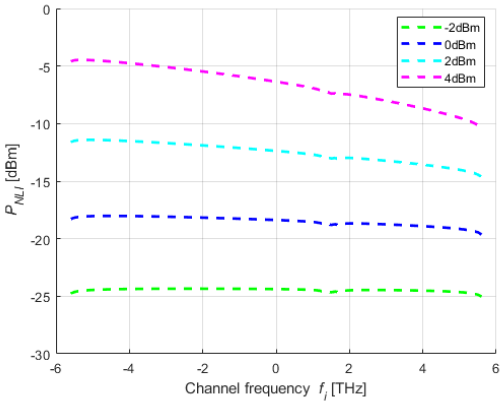

(b)

Figure 9: NLI parameter and p_{NLI} as a function of the channels frequency after nine 10 km spans considering coherent NLI accumulation, for several input powers per channel.

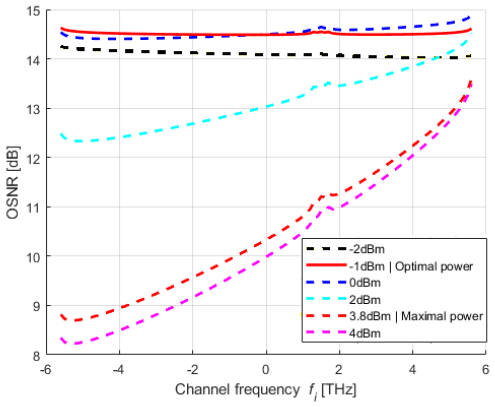

(a)

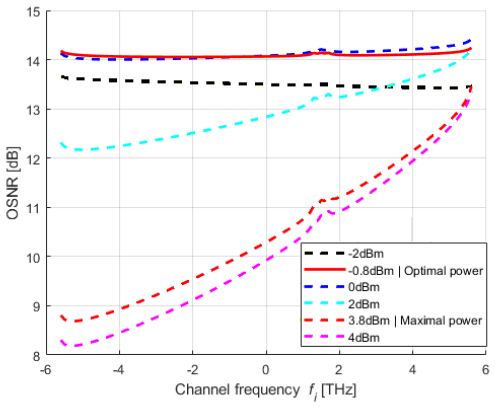

(b)

Figure 10: OSNR as a function of the channel frequency after 9 spans considering the ASE noise power and NLI, for several input channel powers and insertion channel in the (a) tributary node A and (b) hub node 1.

for the worst channel. Fig. 10 corresponds to the case of: (a) channel insertion at the tributary node A and (b) channel insertion at the hub node 1. The OSNR is calculated using Eq. (1).

As can be seen in Fig. 10, for the input power per channel of -2 and 0 dBm, the NLI power tilt has practically no influence, so an almost constant OSNR along all channels is observed. For input powers higher than 0 dBm, we observe that the OSNR increases as the channel frequency increases due to the higher NLI power contribution to the OSNR slope variation. So, we can state that there is an input channel power that gives an optimum OSNR. This optimum OSNR is obtained by evaluating the best possible OSNR, with the highest flatness along the WDM signal bandwidth (slope as close to zero as possible). Hence, the optimal input power that leads to the best OSNR is -1 and -0.8 dBm, respectively, in Fig. 10 (a) and (b), corresponding to the optimal OSNRs of 14.5 and 14 dB. It can be observed that the optimal OSNR is practically constant along frequency ensuring the same received quality for all WDM channels. When the signal is inserted in the hub node, the optimum OSNRs are around 0.5 dB lower than in the case of channel insertion in the tributary node due to the higher ASE noise power added by the hub node.

Finally, it can be observed that all channel powers considered in Fig. 10 comply with the 8.5 dB minimum OSNR required, except for the input power of 4 dBm, where this value is not achieved in the lowest channel frequencies. The maximum input power that ensures the minimum OSNR for all WDM channels is also represented in Fig. 10 and corresponds to 3.8 dBm, for both cases of channel insertion. Therefore, the difference between the optimal OSNR and the minimum OSNR is at least 5.5 dB higher, which ensures enough margin to include other PLIs. For example, if we consider a minimum system margin of 3 dB and an extra power penalty due to other transmission effects of 1.5 dB, like components aging, the minimum OSNR is still accomplished.

4.4 In-band crosstalk in the unamplified solution

In this subsection, the analysis of PLIs, considering the signal transmission in the L-band in a horseshoe topology based on tributary nodes with the FD&W unamplified solution is performed. In this scenario, the main PLI is the in-band crosstalk that arises due to the wavelength reuse in these networks. First, we present the analytical formalism used to assess the impact of this phenomenon, based on the electrical SNR at the receiver output. We start our analysis by presenting the SNR at the receiver output without in-band crosstalk (Rizzelli et al., 2021), and assess the maximum number of spans a signal can cross in a lightpath of the horseshoe topology. After, we introduce the in-band crosstalk in our formalism and assess the respective degradation in terms of the number of spans.

The SNR without in-band crosstalk is given by (Rizzelli et al., 2021)

$$snr = \frac{p_{Rx}}{\frac{\sigma^2_{th}}{P_L^{CW}} + P_L^{CW}\sigma^2_{nLO}CMRR + \sigma^2_{shot} + \frac{p_{Rx}}{SNR_q}} \quad (7)$$

where P_L^{CW} is the continuous wave optical power of the local oscillator (LO), $CMRR$ is the Common Mode Rejection Ratio of the balanced photodetector, SNR_q is an additional term to include several implementation penalties occurring in a coherent system, σ^2_{th} is the variance of the transimpedance amplifier thermal noise (TIA), σ^2_{nLO} is the variance of the LO transmitter relative intensity noise (RIN) and σ^2_{shot} is the variance of the shot noise. The variances σ^2_{th}, σ^2_{nLO} and σ^2_{shot} are given, respectively, by (Rizzelli et al., 2021) $\sigma^2_{th} = \frac{i^2_{TIA}\cdot B^{RX}_{eq}}{8\cdot R^2_\lambda}$; $\sigma^2_{shot} = \frac{q\cdot B^{RX}_{eq}}{2\cdot R_\lambda}$; $\sigma^2_{nLO} = RIN\cdot\frac{B^{RX}_{eq}}{2}$, where R_λ is the overall responsivity of the coherent receiver (considering also the passives losses before the photodiodes), i_{TIA} is the input-referred noise current density of a TIA, B^{RX}_{eq} is the the receiver effective noise bandwidth, q is the electron charge and RIN is the LO RIN parameter. The parameters used to calculate the SNR are based on the fitting to experimental results and are given in (Rizzelli et al., 2021). Only a different symbol rate of 26.75 Gbaud is considered.

In Fig. 11, the BER as a function of the received signal power for different local oscillator powers is presented, considering QPSK modulation, and obtained from the SNR calculated from Eq. 7. The required target BER assumed for the system is 4×10^{-3} (HD-FEC) or 2×10^{-2} (SD-FEC) (Rizzelli et al., 2021). As observed in Fig. 11, for each LO powers of 6, 10, 14 and 18 dBm, the minimum received power required to achieve the target BER is -36.1, -35.7, -35.6 and -33.8 dBm, respectively, for HD-FEC and -38.9, -38, -37.9 and -36 dBm for SD-FEC, which leads to at least 2.2 dB of power budget improvement for SD-FEC in relation to HD-FEC.

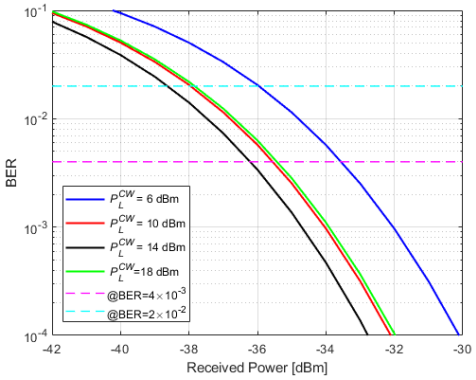

Figure 11: BER as a function of the received signal power for different local oscillator powers P_L^{CW}, for QPSK signals.

From Fig. 11, it can also be observed that the LO power of 14 dBm leads to the minimum received power that ensures the target BER, while $P_L^{CW} = 6$ dBm leads to the higher and most demanding received power to reach the same target BER. Hence, in the following results, we consider $P_L^{CW} = 14$ dBm, as the optimum LO power that leads to the target BER. So, knowing the minimum received power, the main goal is to compute the maximum power budget and the maximum reach of the horseshoe network with an unamplified solution, considering 10 km spans and a reference input power of 0 dBm, taken from the maximum input power considered in (Rizzelli et al., 2021). The maximum power budget is, therefore, 36.1 dB and 38.9 dB, respectively for the HD-FEC and SD-FEC.

Then, the insertion losses per span for hub-span-tributary, tributary-span-hub and tributary-span-tributary transmission, as shown in Fig. 12, are computed.

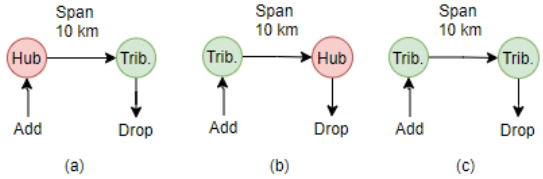

Figure 12: Possible span configurations considered to evaluate the performance of the unamplified solution.

In Tab. 3 are shown, the insertion losses considering the configurations of Fig. 12 for different S/C

dimensions are shown. Note that, the green values are the ones that are feasible for each configuration. As can be seen in Tab. 3, by comparing the power budgets and the insertion losses of just one span with S/Cs 1:16, it can be concluded that the power budgets are not sufficient to accommodate these insertion losses. A possible solution to decrease the insertion losses per span is to reduce the S/C dimension in the A/D structures. So, in the tributary nodes shown in Fig. 4, the S/Cs 1:16 are replaced by S/Cs with smaller size, as considered already in some works (Emmerich et al., 2020b), (Emmerich et al., 2020a), for the unamplified solution. The associated insertion losses are shown in Tab. 3. The A/D structure of the hub node remains the same as in the amplified scenario.

Table 3: Insertion losses considering the configurations of Fig. 12 for different S/C dimensions in the A/D structure of the tributary node.

Total ILs [dB]	S/C 1:2	S/C 1:4	S/C 1:8	S/C 1:16
Hub-span-trib.	36.1	39.1	43.1	47.1
Trib.-span-hub	32.1	35.1	39.1	43.1
Trib.-span-trib.	19.7	25.7	33.7	41.7

It can be concluded that one span is possible with S/Cs 1:2 for the configurations of Fig. 12, whereas only the tributary-span-hub and tributary-span-tributary configurations are possible for S/Cs 1:4, and, for the S/C 1:8, only the tributary-span-tributary configuration is possible. Two spans transmission is not possible.

In order to take into account the impact of in-band crosstalk, the SNR given by Eq. (7) is rewritten as,

$$snr = \frac{p_{Rx}}{\frac{\sigma^2_{th}}{P_L^{CW}} + P_L^{CW}\sigma^2_{nLO}CMRR + \sigma^2_{shot} + \frac{p_{Rx}}{SNR_q} + p_{xc}} \quad (8)$$

where p_{xc} is the crosstalk power defined as $p_{xc} = X_c \times p_{rx}$, with X_c the crosstalk level.

In Fig. 13, the BER as a function of the received signal power with different crosstalk levels is shown. The BER without crosstalk is also represented for comparison purposes. We have considered P_L^{CW}=14 dBm since it leads to the lowest received optical signal power. So, for an input signal power of 0 dBm, and considering the insertion losses shown in Tab. 3, for S/Cs 1:2, 1:4 and 1:8, when the crosstalk level ranges between -35 and -25 dB, the optical power budget is still feasible for all cases assuming a BER=2×10^2 (SD-FEC). For X_c=-20 dB, the minimum received power is about -37.4 dBm, considering SD-FEC, leading to 1.5 dB degradation in relation to the case without crosstalk. Although the optical power budget is reduced, the unamplified solution is still feasible for all the configurations in Fig. 12 for one span. For a 2 spans transmission, the most feasible configuration is tributary-span-tributary due to its lower insertion losses, which are very close to the highest power budget.

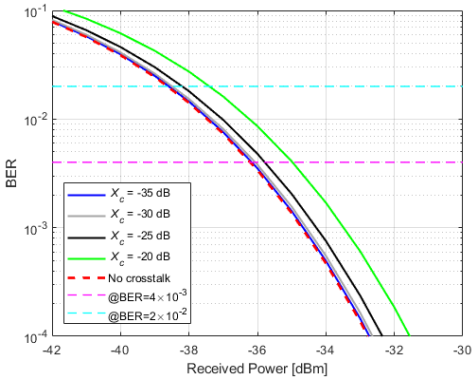

Figure 13: BER as a function of the received signal power with the crosstalk level as a parameter.

5 CONCLUSIONS

In this work, the L-band tributary node architectures known as FD&W with amplified and unamplified solutions have been studied analytically. The hardware components, cost, power consumption, offered capacity and the main PLIs that impair the transmission performance in such nodes have been studied,

When the L-band components cost is twice the C-band cost, the L-band hub and tributary nodes cost is 3.5 times higher than the corresponding C-band node cost. The transponders contribute around 99% to the node final cost.

For the amplified solution, considering an horseshoe network with 2 hub nodes, tributary nodes, and 10 km spans, and two worst path cases of signal transmission, the optimum OSNR achieved at the optical receiver input is above 14 dB, when ASE noise and NLI are considered. This leaves enough margin to guarantee the minimum OSNR in the amplified solution.

In unamplified solutions, to accomplish the power budget, smaller S/Cs 1:2 and 1:4 must be used in the A/D structure of the tributary nodes, and transmission should not exceed one fiber span. This allows frequency reuse in the horseshoe network, leading to in-band crosstalk. For the crosstalk level of -20 dB, a 1.5 degradation on the optical power budget is observed.

ACKNOWLEDGEMENTS

This work was supported under the project of Instituto de Telecomunicações UIDB/50008/2020.

REFERENCES

Agrawal, G. (2010). Fiber-optic communication systems. *New York: Wiley, 14th ed.*

Correia, B. et al. (2021). Power control strategies and network performance assessment for C+L+S multiband optical transport. *Journal of Optical Communications and Networking*, 13:147–157.

Emmerich, R. et al. (2020a). Capacity limits of C+L metro transport networks exploiting dual-band node architectures. *Optical Fiber Communication Conference (OFC) 2020, OSA Technical Digest (Optical Society of America, 2020).*

Emmerich, R. et al. (2020b). Dual-band node architectures for C+L-band capacity upgrades in optical metro transport networks. *21th ITG-Fachtagung*.

Ferrari, A. et al. (2020). Assessment on the achievable throughput of multi-band itu-t g.652.d fiber transmission systems. *Journal of Lightwave Technology*, 38:4279–4291.

Fiberdyne labs, i. (2021). C and C/L band WDM filters.

Hernandez, J. A. et al. (2020). Comprehensive model for technoeconomic studies of next-generation central offices for metro networks. *Journal of Optical Communications and Networking*, 12:414–427.

Inc., T. F. O. A. (2019). Testing fiber optic couplers, splitters or other passive devices. *Available: www.thefoa.org/tech/ref/testing/test/couplers.html*.

Paolucci, F. et al. (2020). Disaggregated edge-enabled C+L-band filterless metro networks. *Journal of Optical Communications and Networking*, 12:2–12.

Rizzelli, G., Nespola, A., Straullu, S., Forghieri, F., and Gaudino, R. (2021). Scaling laws for unamplified coherent transmission in next-generation short-reach and access networks. *Journal of Lightwave Technology*.

Sambo, N., Ferrari, A., Napoli, A., Costa, N., Pedro, J., Sommerkorn-Krombholz, B., Castoldi, P., and Curri, V. (2020). Provisioning in multi-band optical networks. *Journal of Lightwave Technology*, 38:2598–2605.

Semrau, D. et al. (2018). The Gaussian noise model in the presence of inter-channel stimulated raman scattering. *Journal of Lightwave Technology*, 36:3046–3055.

Semrau, D., Killey, R., and Bayvel, P. (2019). A closed-form approximation of the Gaussian noise model in the presence of inter-channel stimulated raman scattering. *Journal of Lightwave Technology*, 37:1924–1936.

Sequeira, D., Cancela, L., and Rebola, J. (2021). CDC ROADM design tradeoffs due to physical layer impairments in optical networks. *Optical Fiber Technology*, 62:102461.

Telecommunication Standardization Sector of ITU, I.-T. R. G. (Oct. 2020). Spectral grids for WDM applications: DWDM frequency grid.